Nanoscale

Single Molecule Raman Spectra of Porphycene Isotopologues

Sylwester Gawinkowski,[a‡] Maria Pszona,[a‡] Alexandr Gorski,[a] Joanna Niedziółka-Jönsson,[a] Izabela Kamińska,[a#] Wojciech Nogala,[a] and Jacek Waluk [a, b]

[a] *Institute of Physical Chemistry, Polish Academy of Sciences, 01-224 Warsaw, Kasprzaka 44/52, Poland;* [b] *Faculty of Mathematics and Science, Cardinal Stefan Wyszyński University, Dewajtis 5, 01-815 Warsaw, Poland.*

[#] Present address: *Institute of Physics, Faculty of Physics, Astronomy and Informatics, Nicolaus Copernicus University, 87-100 Toruń, Grudziądzka 5, Poland.*

ABSTRACT

Single molecule surface-enhanced resonance Raman scattering (SERRS) spectra have been obtained for parent porphycene (Pc-d_0) and its deuterated isotopologue (Pc-d_{12}), located on gold and silver nanoparticles. Equal populations of "hot spots" by the two isotopologues are observed for 1:1 mixtures in the higher concentration range of the single molecule regime (5×10^{-9} M). For decreasing concentrations, hot spots are preferentially populated by undeuterated molecules. This is interpreted as indication of a lower surface diffusion coefficient of Pc-d_{12}. Photostability of single Pc molecules placed on nanoparticles is strongly increased in comparison with polymer environments. *Trans* tautomeric species dominate the spectra, but the analysis of time traces reveals transient intermediates, possibly due to rare *cis* tautomeric forms.

1

Undoubtedly, one of the most spectacular successes in chemistry in the last two decades has been development of the possibility to monitor the behavior of a single molecule. This was achieved through use of various optical and scanning microscopies. The former were initially based on fluorescence. However, using a combination of electronic resonance and surface enhancement it has been demonstrated that even the Raman spectra of a single molecule can be obtained.[1, 2] This observation has spurred the rapid development of surface-enhanced Raman scattering (SERS) techniques and opened up the new, fast-growing field of single molecule Raman (SMR) spectroscopy. The list of molecules for which the SMR spectra have been claimed to have been registered now includes over thirty compounds. Further development was achieved when single molecule Raman technique was combined with scanning probe microscopy, which lead to single molecule tip-enhanced Raman spectroscopy (TERS).[3-7] An impressive achievement has been the real time observation of vibrations of a single molecule located inside a gold dumbbell antenna using coherent anti-Stokes Raman scattering.[8]

In this work, we report and analyze the SMR spectra of porphycene (Pc, Scheme 1), a constitutional isomer of porphyrin. Porphycenes have been a subject of intense investigations since the synthesis of the parent compound was reported in 1986.[9] Among these, studies devoted to spectral and photophysical properties are particularly important.[10-12] Porphycenes are very promising as agents in photodynamic therapy,[13] the main, but not the only theme of numerous patent applications. Other examples of possible use of porphycenes in the areas involving interaction with light include fluorescence immunoassays, tissue marking, optical recording media, and photovoltaic cells. However, fundamental research on these subjects has been rather limited.

The choice of porphycene for single molecule Raman studies was dictated by several factors. First, this molecule has already been observed on a single molecule level using both fluorescence[14-16] and scanning tunneling microscopy (STM).[17-19] Porphycene is a very good model for studying intramolecular double hydrogen transfer.[20-22] The reaction has been thoroughly investigated in condensed phases,[23, 24] supersonic jets,[25-27] and helium nanodroplets.[28] By using polarized light for fluorescence excitation, tautomerization[14, 16] and 3D orientation[15] could be monitored for single molecules. STM investigations of single porphycene molecules placed on a Cu(110) surface showed that

under these conditions, the molecule exists as a previously unobserved *cis* tautomer.[17-19] The *cis-cis* tautomerization could be controlled by placing, with atomic precision, a single copper atom in the vicinity of a single molecule.[18] Thus, a single molecule switch controlled by a single atom was obtained. A natural question arising from this work was whether the single molecules observed using metallic SERS supports correspond to the "normal" *trans* tautomer (as in Scheme 1) or to the "exotic" *cis* species.

<div align="center">Scheme 1</div>

The other goal of this work, relevant for both SMR and fluorescence studies, was to compare the photostabilities of the same single chromophore located in two very different environments: (i) in polymer films used for fluorescence studies; (ii) in "hot spots", i.e., in the vicinity of metal nanoparticles required for the observation of surface-enhanced Raman spectra.

The vibrational structure of porphycene has been studied previously in detail, using not only standard IR and Raman techniques,[29] but also neutron scattering,[29] matrix-isolation,[30, 31] supersonic jets,[27, 32] and helium nanodroplets.[28, 29] Combing these results with theoretical modeling has led to the assignment of 106 out of 108 vibrations.[29] We anticipated that knowledge of vibrational structure can be helpful for single molecule identification and subsequent analysis of temporal evolution of the Raman spectra, in particular in the understanding of the nature of correlations/anticorrelations between various vibrational modes. In addition, the unique polarization characteristics of porphycene - the fact that the molecule can be treated as a "dual dipole" in absorption and emission - make it a very good candidate for single molecule polarization studies, an area that has not been frequently exploited.

We demonstrate that single molecule Raman spectra can be readily obtained for porphycene placed on gold or silver nanoparticles prepared by three different methods: (i) chemical, (ii) electrochemical, (iii) laser ablation. An important difference with regard to the behavior of single molecules in nonmetallic environments, such as solutions or polymers, is a dramatically enhanced photostability. Regarding tautomerization, there is no doubt that *trans* forms are dominant, but time traces of single Raman spectra indicate an infrequent, transient population of *cis* species.

During our studies, we observed an unusual effect which, to the best of our knowledge, has not been reported before: a dramatic change with concentration in the ratio of hot spot populations by two isotopologues: parent porphycene, Pc-d_0, and Pc-d_{12}, porphycene with all peripheral protons substituted by deuterons (see Scheme 1). For 1:1 mixtures at higher concentrations in the single molecule regime, this ratio is (as could have been expected) about 1:1. However, as the concentration is lowered, the ratio increases in favor of the nondeuterated derivative. This is interpreted as being due to different rates of surface diffusion of the two isotopologues. Such behavior may have important implications for single molecule Raman spectroscopy studies, since mixtures of isotopologues are considered ideal systems for implementation of the bianalyte technique, currently the most reliable procedure used to prove a single molecule character of a Raman spectrum.[33-39]

RESULTS AND DISCUSSION

Figures 1 and S1-S5 show the electronic absorption, fluorescence, and the Raman spectra of Pc, the latter obtained for various environments and at different temperatures using four laser lines. By comparing many spectra recorded under different conditions, we wanted to check for the possible presence (in comparable amounts) of more than one tautomeric species. This does not seem to be the case. In general, the Raman spectra obtained with nonresonant excitation (785 nm) and for excitation into S_1 (633 nm), S_2 (514 nm), and into a higher electronic state (325 nm) resemble each other with regard to the number and position of the peaks. The spectra are dominated by totally symmetric A_g modes, but the out-of-plane B_g vibrations are also observed.[29] It is remarkable that, for a particular excitation wavelength, the relative intensities are very similar in both SERS and non-SERS spectra obtained for the chromophore in different environments (crystal, solution, rare gas matrix, gold colloid) and at different temperatures (ranging from 6 to 473 K). On the other hand, significant differences are observed for different excitation wavelengths regarding relative peak intensities. The three resonance Raman spectra resemble each other more in this respect than the spectrum obtained with 785 nm laser. In

particular, the nonresonant spectrum exhibits very weak Raman intensity in the region between 400 and 900 cm^{-1}. A unique feature of the spectra obtained with 633 nm laser line is the observation of overtones and combination bands.

<div align="center">Figure 1</div>

Single molecule spectra. Among various methods used to prove that an observed Raman spectrum corresponds to one obtained from a single molecule, the bianalyte technique is definitely the most reliable.[33-39] In this approach, SERS signals from a mixture of two chromophores are analyzed; for single molecule events, only the spectra corresponding to one or the other component, but not their sum, are obtained. It is considered that an ideal case corresponds to the mixture of two isotopologues, since in this case the electronic spectra are virtually identical, and the vibrational features, although distinctly separated, often lie very close. We applied the bianalyte technique using a mixture of parent, undeuterated molecule (Pc-d_0) and the chromophore deuterated on the periphery (Pc-d_{12}). Figure 2 shows the comparison of the Raman spectra of the two isotopologues in the region between 300 and 400 cm^{-1}. The frequencies of the two bands, corresponding to $3A_g$ and $4A_g$ modes[29] are clearly different; one should also note the inversion in the intensity ratio. Both effects are reproduced by calculations. For samples prepared using 10^{-8} M solutions, we observe both the pure Raman spectra of each component and spectra that show the presence of both isotopologues (Figure 2, top). The statistics change when the concentration is lowered to 10^{-10} M (Figure 2, bottom). Now, the spectra correspond to either Pc-d_0 or Pc-d_{12}, strongly suggesting that the single molecular regime has been reached. This is confirmed in Figure 3, which presents histograms of "one-chromophore" vs. "both chromophores" events, obtained for different concentrations in the stock solution. From this data, the upper limit of concentration required for single molecule Raman measurement can be estimated as 5×10^{-9} M. At the border between the two regimes, one often observes events involving a small number of chromophores, as can be deduced from the analysis of time traces (Figure S6).

<div align="center">Figures 2-3</div>

A spectacular change in the shape of the event histogram is observed when the concentration of Pc-d_0 and Pc-d_{12} in the 1:1 mixture is decreased further. Now, the single molecule events involving the nondeuterated porphycene become much more frequent than those for Pc-d_{12} (Figure 3). Since the statistics become less reliable upon decreasing the concentration, and thus the number of observed events, we repeated the measurements many times using different supports and different methods of sample preparation (drop casting as well as immersion in chromophore solution). All these approaches yielded the same pattern of lower probability of observing Pc-d_{12} as the concentration decreased. Only at the higher end of the single molecule regime was the ratio of single molecule events for each isotopologue close to 1:1, with only a slight predomination of Pc-d_0.

If the above effect were due to different enhancement factors, different absorption coefficients, or different affinity towards hot spots in the two isotopologues, the same ratio should have been observed for all tested concentrations. However, this was not the case. The significantly lower ratio of single molecule Pc-d_{12} events with respect to Pc-d_0 at lower concentration may be explained by a difference in diffusion coefficients of the two isotopologues. This difference becomes detectable only when the average occupation number of a hot spot is very low and the molecules "compete" for hot spots by diffusion on the surface of metal nanostructures. Such conditions are achieved in the low concentration regime.

Similar histograms were observed for different SERS substrates, although the limit of the single molecule regime was slightly shifted, most likely due to different hot spots densities and/or surface wettability, which, in turn, resulted in an alternation of the concentration of the dye on the surface. We did not detect a trend related to the number or distance between hot-spots: this conclusion is based on similar changes of histograms with concentration observed for very different supports.

Different populations of the isotopologues in hot spots are not caused by "coffee ring effects".[40] If that were the case, one would expect to observe maps dominated by Pc-d_0 in certain spatial regions as well as, for different regions, maps with prevailing Pc-d_{12} population. Only the former have been detected.

We also obtained evidence that once the hot spot is populated, the molecule, independent of isotopic substitution, can remain there for a long time (minutes to hours, e.g., Figure 6A). This is true for both illuminated and non-illuminated regions, as demonstrated for the former by time traces lasting for minutes and, for the latter, by recording a series of maps (up to several hundred) of the same spectral regions. Many of the hot spots survived over the course of such experiments.

The motional properties of isotopologues of single molecules on surfaces have not been intensely investigated so far. Differences in rotational statistics have been reported for acetylene isotopologues adsorbed on a Cu(100) surface at 8 K.[41] Porphyrins are known to be quite mobile on metal surfaces, although differences between free base and metal complexes are significant.[42-46]. Diffusion is usually analyzed using an Arrhenius model. Expressing diffusion in terms of activation energy involves a term which may be different for Pc-d_0 and Pc-d_{12} because of the difference in zero-point energies. Lower energy, and thus a smaller exponential term is naturally expected for the multiply deuterated species.

An independent proof of the single molecule character of the spectra was obtained using the bianalyte technique for a 1:1 mixture of Pc-d_0 with Nile blue, a dye for which the single molecule Raman spectra have been reported.[39, 47-49] The relevant histograms are shown in Figure S7. In addition, such procedure allowed comparing the relative intensities of the Raman bands from single Pc and Nile blue molecules. The intensities of the Nile blue band at 592 cm^{-1} and Pc-d_0 band at 343 cm^{-1} recorded in the single molecule regime with 633 nm laser line were compared with the results obtained for acetone solutions of the same chemicals using 785 nm excitation. Taking into account differences in concentration and absorption coefficients, the relative enhancement was about 30 times stronger for porphycene. One should note, however, that the onset of electronic absorption in Nile blue (700 nm) is closer to 785 nm than in porphycene, and therefore the Raman intensity of the former may be more strongly enhanced by the preresonance effect. A proper comparison of the enhancement factors (EFs) for the two chromophores would require longer excitation wavelengths.

The map shown in Figure 2 consists of 3355 points. Out of those, only 30 exhibit SM Raman spectra. Such behavior was approximately the same for different homemade NP support.The commercially available nanorods had a higher density of hot spots.

The spectra exhibit features characteristic for the single molecule regime: blinking and bleaching. Figure 4 shows a time trace of the intensity of the 343 cm^{-1} (3A$_g$) mode of Pc-d_0. Large intensity fluctuations are observed prior to a sudden drop, i.e., bleaching of the molecule. Interestingly, the difference between blinking and bleaching is not always well defined, as recovery of intensity has sometimes been observed after very long "off" periods (tens of seconds). It is possible that in such cases the reappearing signal stems from another molecule. However, our attempts to prove this by showing an SMR spectrum that changes from that of Pc-d_0 to that of Pc-d_{12} (or *vice versa)* in series of spectra registered from the same sample point were not conclusive. Such behavior was observed only in a few time traces out of many hundreds. What we did observe was the formation and disappearance of Raman signals at different points of the sample in the series of maps recorded for the same area over a period of tens to hundreds of seconds (Figure S8). Another typical feature is the variability of the relative peak intensities in the spectra registered from different hot spots (Figure S9). In general, the largest differences in intensity are observed between the low and high frequency regions, but a detailed analysis indicates large variations also for peaks located close to each other (e.g., the two intense bands at around 1330 and 1390 cm^{-1}). On the other hand, the averaged SM spectra obtained from different supports are remarkably similar. They also do not change significantly as the temperature is lowered, although the bands become narrower (Figure S10) and the intensity fluctuations decrease.

Figure 4

Dependence on support. Reliable comparison of different SERS supports is not an easy task, due to their heterogeneous nature. Depending on the ultimate purpose of particular study or application, various quality criteria may be considered, e.g., spectral intensity, reproducibility, uniformity, density of hot spots, sample stability, purity, etc. A general conclusion from our investigations is that Raman spectra of single porphycene molecules

can be readily obtained for each type of support we studied (Figure 5), provided that the excitation wavelength is 633 nm. Attempts to obtain the SM spectra using three other laser wavelengths were not successful. For 633 nm, we have observed single molecule spectra for each kind of gold and silver NPs we used. The spectra were obtained not only for solid supports, but also in colloid suspensions (Au and Ag). On the other hand, large variations were observed between different batches of the same type. Therefore, in order to make at least a semi-quantitative comparison between different supports, we selected those that gave the best results in their class for analysis. Among all tested SERS substrates, gold nanorods turned out to be the best with respect to the density of hot spots and enhancement factors. Highly disordered, fractal-like configurations of nanorods ensure a high density of hot spots, while a broad macroscopically measured plasmon band indicates a high number of hot spots with individual plasmon resonances spectrally close to the excitation laser line. These substrates have proven not only to be the best for SMR spectra detection using 633 nm excitation, they also exhibited the highest EFs for measurements with 785 nm excitation. This enabled recording of SERS spectra for low concentrations of Pc in solution (down to 10^{-7} M).

Figure 5

SMR substrates should also be as chemically pure as possible. In particular, they should be free from easily SERS-detectable substances, which may give artificial bands interfering with the analyte spectra. Impurities can also occupy hot spots, thus blocking the access of the analyte molecule. From this point of view, the substrates obtained without use of any chemicals other than water and metal during preparation ensure minimal chance of misinterpretation of the SMR results. The substrates based on Ag and Au nanoparticles obtained by laser ablation in water were the best in this respect. The other nearly spectrally clean substrate was made by electrorefining of microelectrode. During this process, NaCl solution was used as an electrolyte. NaCl does not give SERS spectra even at high concentrations and is highly soluble in water, so it could be nearly completely removed by simple immersion in clean water. Despite the cleanliness of these preparation methods, some sporadic, but intense artificial SERS spectra were observed

for both types of substrates. One cannot exclude that these spectra might be due to substances present in air and, to completely avoid such artifacts, the whole procedure of sample preparation and measurements should be performed in a chamber with a fully controlled environment.

Enhancement factor estimation. The enhancement factor (EF) was estimated according to the definition and procedure described in the literature.[49] The EF is defined as the ratio of SERS (I_{SERS}) and Raman (I_{Raman}) signal intensities:

$$EF = (I_{SERS}*N_{Raman})/(I_{Raman}*N_{SERS}) \qquad (1)$$

These intensities must be normalized by the factors influencing the registered intensities: (a) the number of molecules involved (N_{Raman}/N_{SERS}) and (b) the excitation powers (P_{Raman}/P_{SERS}), if they are different in both types of measurements.

Despite the simple definition of EF, the estimation of its value is a challenging task. Usually, only I_{SERS} can be easily measured. In the case of SERS signal coming from a single molecule N_{SERS} is by definition equal to one, but N_{Raman} can be only roughly estimated. This value can be defined as the number of molecules in the focal volume of the objective used to measure I_{Raman}. The focal volume is frequently assumed to have the diffraction-limited value, but this is rarely the case in real experiments, and the effective focal volume should be estimated experimentally. The effective focal volume was determined by lateral mapping and then depth profiling of fluorescent nanospheres with 100 nm step. Contrary to the earlier proposed cutting-edge knife method[49, 50] on a silicon wafer, the simple procedure proposed here allows estimation of the effective focal volume without assuming that the exciting and detecting foci are the same.

The most precise estimation of the number of molecules in the focal volume can be made using a non-absorbing liquid or a solution with uniformly distributed solute molecules. Unfortunately, the 633 nm laser line is very close to the 0-0 transition in Pc and, as a result, both the fluorescence maximum and the Raman bands lie in the same spectral range. Because the absorption coefficient of Pc is quite high (~50000 $M^{-1}cm^{-1}$) and the fluorescence quantum yield of Pc is also significant (0.36-0.49, depending on

solvent), the resonance Raman spectrum is overlapped by fluorescence many orders of magnitude higher. In principle, using polarization techniques combined with long accumulation, it is possible to determine the resonance Raman cross sections even for cases where a weak Raman signal lies on top of a strong emission.[51-53] Such method was recently successfully applied to extract Nile blue and rhodamine 6G (R6G) Raman spectra from a strong fluorescence background.[51, 52] Unfortunately, unlike in R6G, where the measured Raman bands lie on the tail of its fluorescence, in the case of Pc excited with a 633 nm laser line the Raman bands appear exactly on top of the fluorescence band. Therefore, even collecting a very high number of acquisitions, with total time of accumulation above 78 h, was not enough to distinguish Raman features from noise.

In this situation it was necessary to use a Pc crystal as a not surface-enhanced reference sample. The strong fluorescence of Pc appears for monomers in solution, but is significantly quenched and red-shifted for dimers and higher order aggregates, of which the extreme case is the monocrystal. It was possible to distinguish the first three RR bands on the uphill side of the fluorescence band. Additionally, we observed that decreasing the temperature causes an additional red shift of the luminescence band (Figure S11). Between 123 and 223 K, the emission is shifted to the red, thus exposing the Raman spectrum in a background-free range of about 1000 cm^{-1}. An even wider range resonance Raman spectrum, up to 1700 cm^{-1}, was measured at room temperature from a thin polycrystalline film of Pc, prepared by smearing the compound between two glass microscope slides. The effective number of Pc molecules contributing to the registered I_{Raman} signal was estimated on the basis of such a measurement. The number of molecules in the laser focus volume was calculated using X-ray data on crystal density. Because of the strong absorption of the Pc crystal at 633 nm (Figure S12) this number was scaled down by assuming it has the same absorption coefficient as in solution. The number of molecules contributing to the signal is slightly overestimated, since we did not include a different refractive index for the crystal.

Based on this procedure, we obtained a SERS enhancement factor of about 10^{11} for the "hottest" SM events and ~10^9 for the lowest detectable ones. The integral intensity of the 343 cm^{-1} band (usually being the strongest in the SERS spectra) was used in the calculations. The highest (10^{11}) value of EF was registered only for a few molecules; it is

in agreement with the highest previously observed EF,[54] as well as with predictions made by calculations.[55-57]

An estimation of the resonance Raman enhancement factor (EF_{RR}) was also performed, by comparison of intensities of the 343 cm^{-1} band measured for the 633 nm (resonance Raman) and 785 nm excitations. Both measurements were performed for the monocrystal. Taking into account the ν^4 factor, a value of $EF_{RR}=10^3$ was estimated. This value should be considered a lower limit, since the excitation at 785 nm corresponds, for the crystalline Pc in particular, to the pre-resonance Raman regime.

Detailed information concerning estimation of the enhancement factors can be found in the Supporting Information.

Raman and fluorescence spectra. It is remarkable that SM Raman spectra can be observed for porphycene using 633 nm excitation, a wavelength that is close to the first absorption maximum. The fluorescence of Pc exhibits a very small Stokes shift of a few nanometers and strongly overlaps with the Raman spectrum. This situation makes the registration of SMR more challenging for Pc than, e.g., R6G, crystal violet, or Nile blue, which exhibit Stokes shifts of 30, 35, and 35 nm, respectively. Moreover, the fluorescence quantum yield of Pc in solution is very large (0.36-0.49 at 293 K in different solvents). Still, the SM Raman spectra were usually stronger than fluorescence, although the emission was observed as a background. The spectral shape of the fluorescence was typical for porphycene. Most importantly, temporal intensity profiles were the same for fluorescence and Raman, indicating that both come from the same single chromophore. This behavior was observed for Pc-d_0 and Pc-d_{12} on solid supports (Figure 6A-C) and in solution (Figure 6D), for longer (Figure 6A and 6C) and shorter (Figure 6B) time scales. We did not observe the so-called "white background" emission, often reported in the literature.[58-63]

Figure 6

Evidence for two tautomeric forms. Ample experimental evidence shows that porphycene exists in the *trans* tautomeric form in solutions, glasses, and polymers,[11, 64] as well as

12

when isolated in supersonic jets,[26, 27] helium nanodroplets[28] or rare gas matrices.[31] However, the STM studies carried out for single porphycene molecules located on the (110) surface of copper monocrystals demonstrated that under these conditions Pc exists in the form of two chemically equivalent, interconverting *cis* tautomers.[17-19] Therefore, we expected a possibility of finding this rare tautomeric form for Pc located on gold or silver surfaces. There is no doubt that for most of the SM spectra recorded on different substrates *trans* Pc is the observed chromophore. However, in rare instances we did observe reversible changes in consecutive spectra that suggest *trans-cis-trans* tautomerization. This is shown in Figure 7, where we compare the SM Raman spectra with quantum-chemical simulations of Raman activity for both species. The theory predicts that the strong Raman band appearing at 180 cm^{-1} in the *trans* form of both isotopologues should be blue-shifted by about 20 cm^{-1} in the *cis* species, whereas the frequencies of other low energy modes should be essentially unchanged. This is exactly the behavior observed in the experimental curves. Another prediction, corroborated by experiment is the appearance of a strong transition around 1420 cm^{-1} in the *cis* form of Pc-d_{12}.

Figure 7

The spectral changes that we attribute to tautomerization in single molecules were observed both at 293 K and at low temperatures, suggesting, in accordance with STM studies[17-19] that the process is governed by hot spot structure rather than temperature. For porphycene isolated in supersonic jets or helium nanodroplets, tunneling splittings are observed in the electronic absorption and fluorescence spectra. These splittings, due to a symmetrical double minimum potential for *trans-trans* double hydrogen transfer, are vibrational-mode-specific: the largest values are observed for the $2A_g$ mode, its overtones and combinations with the $3A_g$ and $4A_g$ modes. It is interesting to notice that the SMR spectra clearly reveals that the bandwidths involving $2A_g$ (183 and 179 cm^{-1} in Pc-d_0 and Pc-d_{12}, respectively) and its combinations with $3A_g$ (343 and 327 cm^{-1}) and 4 A_g (367 and 349 cm^{-1}) are larger than those corresponding to $3A_g$, $4A_g$, and most of the other modes. The latter exhibit bandwidths of ca. 6-7 cm^{-1}, due to the spectral resolution of our

instrument, whereas the $2A_g$ related bands are twice as broad (ca. 12-14 cm^{-1}). The latter value coincides with the tunneling splitting of 12 cm^{-1} observed in supersonic jets for both for Pc-d_0 and Pc-d_{12}. It is too early to postulate that the difference in bandwidths is due to mode-selective tunneling splitting in single Pc molecules, but this observation calls for further SMR studies with better spectral resolution.

Photostability. Preliminary experiments carried out for bulk porphycene solutions and for single Pc molecules embedded in polymer sheets indicate that, for irradiation into the Q bands (500-630 nm) the quantum yield of photodestruction is on the order of 10^{-6}. This is not bad; however, in the single molecule fluorescence studies it translates into the observation time of several seconds, after which the molecule bleaches. Our SM Raman spectra can be recorded at comparable laser intensities for much longer: minutes and, in several cases, over an hour. Thus, the photostability of Pc is enhanced by roughly two orders of magnitude when the molecule is placed on a gold or silver surface. A possible reason for enhanced stability is the shortening of the lowest excited singlet lifetime and, as a consequence, low probability of intersystem crossing to the triplet state (which, if formed, would also have a much shorter lifetime). This mechanism is often implicitly or explicitly assumed when reporting enhanced photostability on SERS substrates.[65-71] However, to the best of our knowledge, the possible connection between the chemical enhancement mechanism of SERS and photostability has not been discussed so far. It can be envisaged that charge transfer between the chromophore and substrate may decrease photostability. It was recently reported that the stability of R6G probed by SERS increases when a graphene monolayer is inserted between the substrate and the dye molecule.[72] In this context, one should also note a crucial relationship between photostability and the enhancement factors, as the molecules with highest EFs should be most prone to photobleaching.[73, 74] For these reasons, we believe that the finding of enhanced stability of Pc is not trivial, especially when compared to the parent isomer, porphyrin. Our attempts to register SM Raman spectra from porphyrin were not successful: the spectra obtained differed from those of free base porphyrin, most probably due to the metal insertion into the inner cavity. This effect has been reported before.[75] The difference in stability between the two isomers is caused by two intramolecular

NH···N hydrogen bonds, much stronger in porphycene. As a result, metallation of porphycene is much less probable.

SUMMARY AND CONCLUSIONS

Porphycene is a unique example of a chromophore that has been investigated on a single molecule level using three different techniques: Raman, fluorescence,[14, 15] and STM.[17-19] The present study demonstrates two advantages of single molecule Raman vs fluorescence. The first results from the obvious difference in spectral resolution, allowing separation of features from various isotopologues or tautomeric forms in the Raman spectra. It should be noted that the fluorescences of *trans* and *cis* tautomers of porphycene are so similar that, even in the favorable case when both forms are present in comparable amounts, the proof of their coexistence is indirect and based on rather complicated emission anisotropy studies.[24]

Second, the enhancement of photostability we observed on nanometallic supports used for SMR is spectacular, enabling observation of a single chromophore over a time 1-2 orders of magnitude longer than when using fluorescence.

Finally, a novel and, somewhat unexpected finding that isotopologues of the same chromophore may populate hot spots with different probabilities may have implications for single molecule studies. On one hand, it may complicates the analysis by the bianalyte method. On the other hand, these differences may be further exploited, e.g., in the studies of hot spots distribution for a particular system.

Due to its stability and well-known vibrational and tautomeric structure, porphycene emerges as a very good model for further single molecule Raman studies. We are currently extending the SMR investigations to assess the effects of temperature, support, polarized excitation, and specific substitution. It should be added in this context that our current library of porphycenes presently includes over fifty differently substituted or modified species, so that the studies initiated for the parent compound can be continued in a systematic fashion. To address a specific problem, one can focus on a specific molecular parameter (size, electronic spectrum, hydrogen bond strength, etc.), varying it in a controlled way. Such an approach has been successful in a recent study of

tautomerization rate-affecting factors in a series of nineteen differently substituted porphycenes.[64]

EXPERIMENTAL DETAILS

Synthesis. Porphycene was synthesized and purified according to procedures described earlier.[76] The deuterated isotopologue (Pc-d_{12}, with all peripheral CH protons replaced by deuterons, see Scheme 1) was obtained as follows: 20 mg of Pc was dissolved in 3 ml of 98% D_2SO_4 (Aldrich, 99.5% deuterated). Then, 1 ml of D_2O (Aldrich, 99.9% deuterated) was added and the solution was kept at 180^0 C in an oil bath for 8 hours. Afterwards, 20 ml of chloroform (Merck, spectroscopic grade) was added to the cooled solution and then the mixture was neutralized by NaOD (Aldrich, 99%+ deuterated)/D_2O 25% solution. After extraction, the product was transferred into an organic phase. The aqueous layer was removed and the organic phase was evaporated in vacuo. This procedure was repeated several times using incompletely perdeuterated porphycene product from the last step as a substrate for the subsequent iteration. Finally, perdeuterated porphycene powder was rinsed several times with D_2O and *n*-hexane to remove polar and non-polar contaminants, respectively. The obtained powder of Pc-d_{14} was found to exchange the inner cavity deuterons with protons while drying, due to water present in the air. The degree of perdeuteration for the final Pc-d_{12} product was verified to be higher than 90% using mass spectrometry with electrospray ionization (ESI-MS).

Synthesis of nanoparticles. Nanoparticles (NPs) were prepared using chemical, electrochemical, and physical methods. Chemical synthesis of silver colloids was performed as described in the literature.[77] Approximately 1 ml of 15 mM hydroxylamine hydrochloride (Aldrich) and 30 mM sodium hydroxide solution were added to 9 ml of 1.1 mM silver nitrate (Merck) solution under rapid stirring. Chemically clean silver and gold colloids were obtained by a laser ablation method. A small bar of gold (Mint of Poland, 99.99%) or a silver wire (Aldrich, 99.9%) were mounted in a quartz cuvette filled with distilled water and irradiated by a focused beam of a pulsed laser. Two types of lasers were used: (i) Lambda Physics LPX100 excimer laser (XeCl, 308 nm) with the energy tuned in the range of 10 – 90 mJ per pulse and with a 25 ns pulse duration; (ii) PL 8000 (Continuum) Nd:YAG operated at the fundamental wavelength (1064 nm) and at the second harmonic (532 nm), with approximately the same energy of 20 mJ per pulse and 10 ns pulse duration for each. The repetition rate of both lasers was 25 Hz, which allowed production of metal colloids with sufficient concentration within a few minutes. All colloids were characterized by measurements of their extinction coefficients.

In addition to the homemade nanoparticles described above, we also used commercial nanoparticles, Nanopartz Bare Gold Nanorodz A12-25-600 and A12-25-650. These gold nanorods have dimensions of 25×47 and 25×60 nm and longitudinal plasmonic resonances in water solution at 600 and 650 nm, respectively. The plasmonic band maximum shifts to 850 nm after deposition on glass and the bandwidth increases significantly, covering a spectral region from about 500 to 1200 nm. The colloidal solution is stabilized by cetyl trimethylammonium bromide (CTAB). Before deposition on glass, the colloid (0.37 nM) was concentrated and excess CTAB was removed by the following procedure: 1 mL of colloid was centrifuged for 10 minutes at 6000 rpm,

decanted, redissolved in 1 mL of water, and again centrifuged. After repeating these steps two times, the final solution was drop cast on a microscopic cover glass and left to dry under ambient conditions.

SM-SERS substrate and sample preparation. A silicon wafer was cut into about 5×5 mm^2 squares and cleaned by bathing for 15 minutes in freshly prepared piranha solution (1:1 mixture of 96% H_2SO_4 and 30% H_2O_2, both from Aldrich), then washed with distilled water, and dried under ambient conditions. The same procedure was used for cleaning glass microscope coverslips. A few drops of gold or silver colloid were then cast on the silicon wafer or on the coverslip and left until dry. The morphology of nanoparticle aggregates was characterized by AFM or SEM techniques. A drop of Pc-d_0 or Pc-d_{12} solution in ethanol (Merck, spectroscopic grade) or 1:1 mixture of the isotopologues was spread using a micropipette on the SERS substrate and evaporated under ambient conditions.

In the first method, the support was obtained by localized electrorefining using scanning electrochemical microscopy. Briefly, a gold microelectrode (100 µm diameter) was positioned and then moved 20 µm above an ITO electrode (tin-doped indium oxide coated glass), both placed in 3M NaCl aqueous solution. The applied voltage induces the electrodissolution of the gold wire and its simultaneous electrodeposition on the ITO electrode. As a result, a thin layer of gold nanostructures is deposited on the ITO surface. By changing the parameters (voltage, distance between electrodes, and gold microelectrode movement velocity) both the morphology and the SERS activity of the structures can be modified.[78]

In the second method, gold nanoparticles were obtained by electrodeposition on an ITO electrode (sheet resistivity 8-12 Ω per square, Delta Technologies Ltd.) at a three-phase junction, as described elsewhere.[79] The ITO electrode was immersed in an electrochemical cell containing two immiscible liquids. The organic phase was toluene (Chempur) which contained 1 mM tetraoctylammonium tetrachloroaurate salt obtained by anion exchange from tetraoctylammonium bromide (98%, Aldrich) in toluene and $HAuCl_4 \cdot 3H_2O$ (98%, Aldrich) in aqueous solution.[80] The second phase was water with 0.1 M KPF_6 used as a supporting electrolyte. A double-step chronoamperometry technique was employed for particle deposition with a nucleation potential V_1 = -1.0 V applied for 50 ms and a growth potential V_2 = 0 V applied for 2500 s.

Instrumentation. A Shimadzu UV 3100 spectrophotometer was used for measurements of the electronic absorption and extinction spectra in the UV/VIS range. The Raman spectral measurements and mapping were done using InVia Renishaw Raman spectrometer with an integrated Leica microscope equipped with thermoelectrically cooled 1024×256 pixels CCD detector and a bright single monochromator. The Raman spectra of Pc crystals and SERS spectra were collected using 100× Leica objective (NA=0.85) and dispersed by 1200 and or 1800 grooves/mm holographic gratings in the visible spectral range. For Raman measurements in liquids and cryogenic matrices, Renishaw objectives with 15, 30, or 60 mm working distance were used. For temperature dependent (77 – 500 K) Raman and SERS measurements the samples were placed in a Linkam THMS600 heating/freezing chamber and a long working distance Olympus 50× objective was used (NA=0.50). In the UV range, a combination of 40× objective

(Thorlabs, NA=0.5) and 2400 grooves/mm holographic grating was employed. Four laser lines were used: 325 nm (He-Cd, Kimmon), 514.5 nm (Stellar Pro argon Modu-Laser, LLC), 632.8 nm (HeNe, Renishaw), and 785 nm (HPNIR785). The use of dielectric cut-off filters allowed registering of Stokes shifts down to 40 cm^{-1} for 514.5 nm excitation, to 100 cm^{-1} for 632.8 and 785 nm excitations, and to 200 cm^{-1} for the 325 nm laser line. For the simultaneous measurements of Stokes and anti-Stokes branches of SERS spectra, a BragGrate notch filter was used, allowing the registration of spectral features located as close as 10-15 cm^{-1} to the 632.8 nm laser line. The spectral resolution in the visible range was 4-6 cm^{-1} depending on the laser line and grating combination. In the UV range the resolution was about 10 cm^{-1}. The wavenumber accuracy was 2 cm^{-1}, which was calibrated after each optical rearrangement with both Rayleigh laser line and the 520.6 cm^{-1} band of silicon crystal. The piezo stage allowed for mapping with 100 nm steps in the horizontal plane and with 200 nm steps in depth. A collection of neutral grey filters allowed laser light power to be controlled at the sample and helped to prevent its thermal decomposition.

Low-temperature argon and xenon matrices of Pc were deposited onto a sapphire window mounted in the CSW-202 N Advanced Research Systems closed-cycle cryostat. An Ntegra NT-MDT atomic force microscope (AFM) and FEI NovaNano 450 scanning electron microscope (SEM) were used for characterization of substrate morphology.

Raman measurements and analysis procedure. The Raman mapping was carried out by raster scanning a sample in the horizontal (XY) plane and registering Raman spectra at each point. Renishaw Wire 3.3 software was used to obtain the map of intensity distribution and to remove contributions from cosmic rays. The temporal evolution of spectra from the selected hot spots was recorded with a time window down to 250 ms. Raman spectra of bulk Pc excited with 325, 514, and 785 nm were registered in a quartz cuvette in toluene, CCl$_4$, and acetone solutions. Raman spectra of Pc crystals were measured with all four laser lines.

Normal mode analysis and geometry optimizations were performed at the density functional theory (DFT) level with the B3LYP functional and 6-31G(d,p) basis set, using Gaussian 09.[81]

ASSOCIATED CONTENT
Supporting Information
Details of estimation of the enhancement factors, additional Raman, SERS, fluorescence, and absorption spectra and maps. This material is available free of charge via the Internet at http://pubs.acs.org.

AUTHOR INFORMATION
Corresponding Author
*E-mail: jwaluk@ichf.edu.pl

Author Contributions
‡These authors contributed equally.

Notes
The authors declare no competing financial interest

18

ACKNOWLEDGMENTS

Scheme 1. Structure of porphycene (*trans* tautomer) and the scheme of deuteration. Left, Pc-d_0; right, Pc-d_{12}.
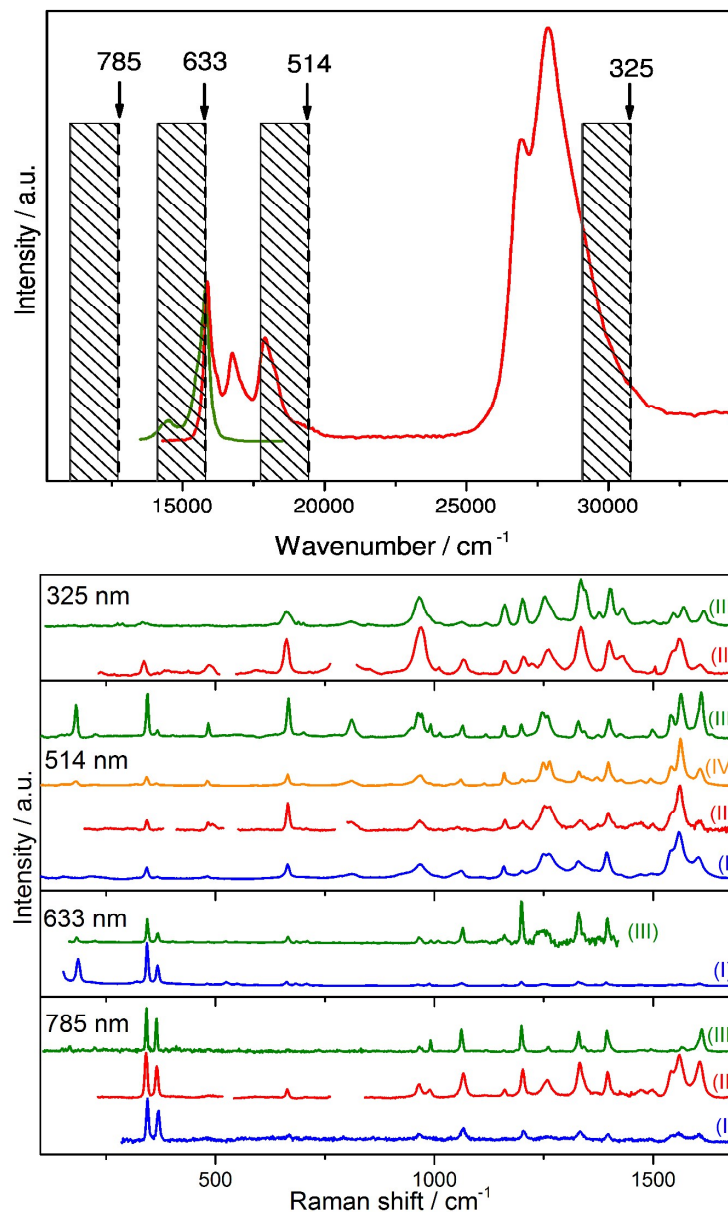
Fig. 1 Top: absorption (red) and fluorescence (green) of Pc-d_0 in tetrahydrofuran at room temperature. Striped bars indicate Stokes Raman regions excited by four different laser lines, with the wavelength indicated by arrows. Bottom: comparison of Raman spectra of Pc-d_0 excited with four laser lines under different conditions: (I) SERS spectra from solid gold nanostructures measured at room temperature for 785 and 514 nm excitation, and at 77 K for 633 nm excitation; (II) Raman spectra in acetone solution recorded at room temperature; (III) Raman spectra of a crystalline sample at 293 K; (IV) Raman spectrum of Pc-d_0 in Xe matrix measured at 6 K.
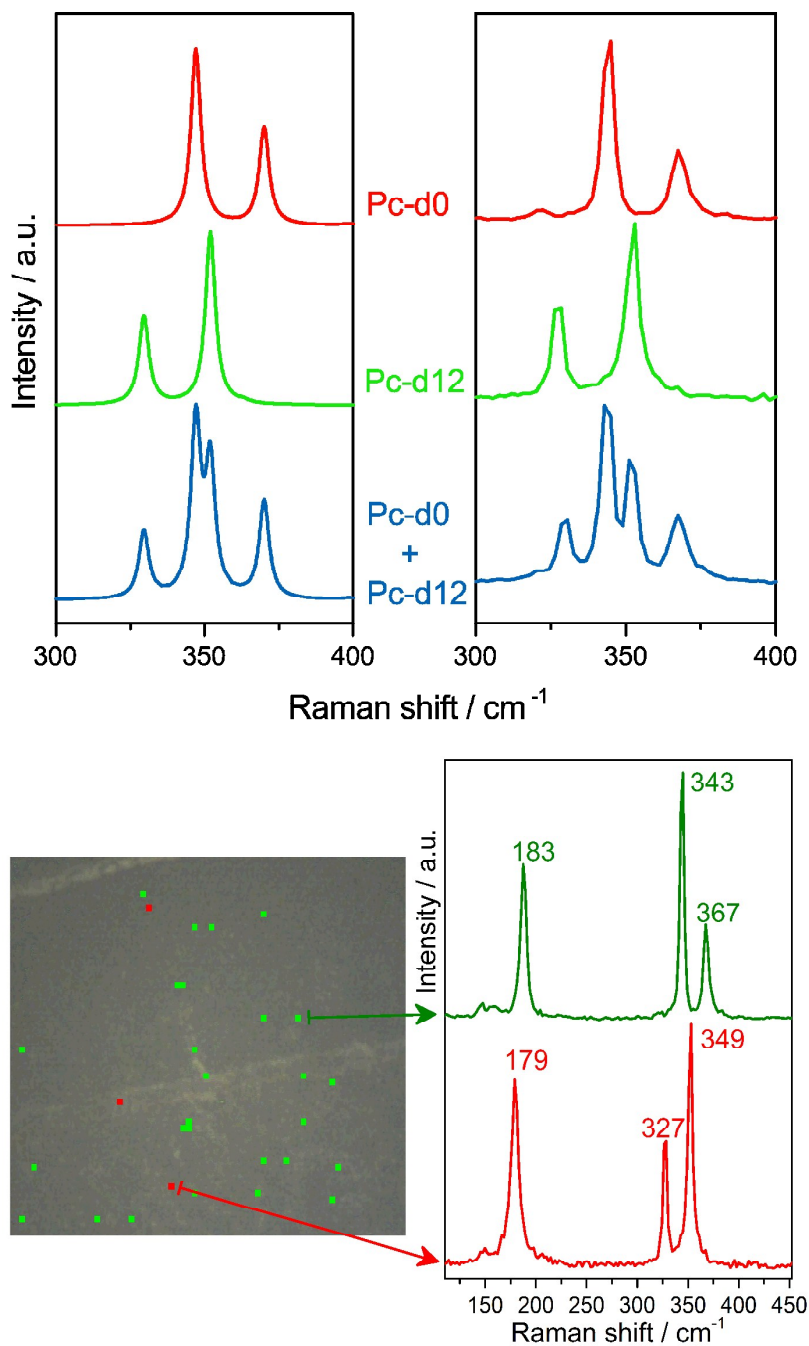
Fig. 2 Top: fragments of SERRS spectra of Pc-d_0 (red), Pc-d_{12} (green), and their 1:1 mixture (blue) obtained from different points of gold NPs/glass substrate (right), compared with the spectra simulated using B3LYP/6-31G** (left). 10^{-8} M ethanol solution was used. Bottom left: 2D map of Raman spectra registered from a 1:1 Pc-d_0:Pc-d_{12} mixture (~5+5 molecules/μm^2, 10^{-10} M solution) deposited on a gold NPs/glass substrate. The points for which the spectra correspond exclusively to Pc-d_0 and Pc-d_{12} are shown as red and green squares, respectively. Bottom right: SM-SERRS spectra obtained from two different hot spots on the map.
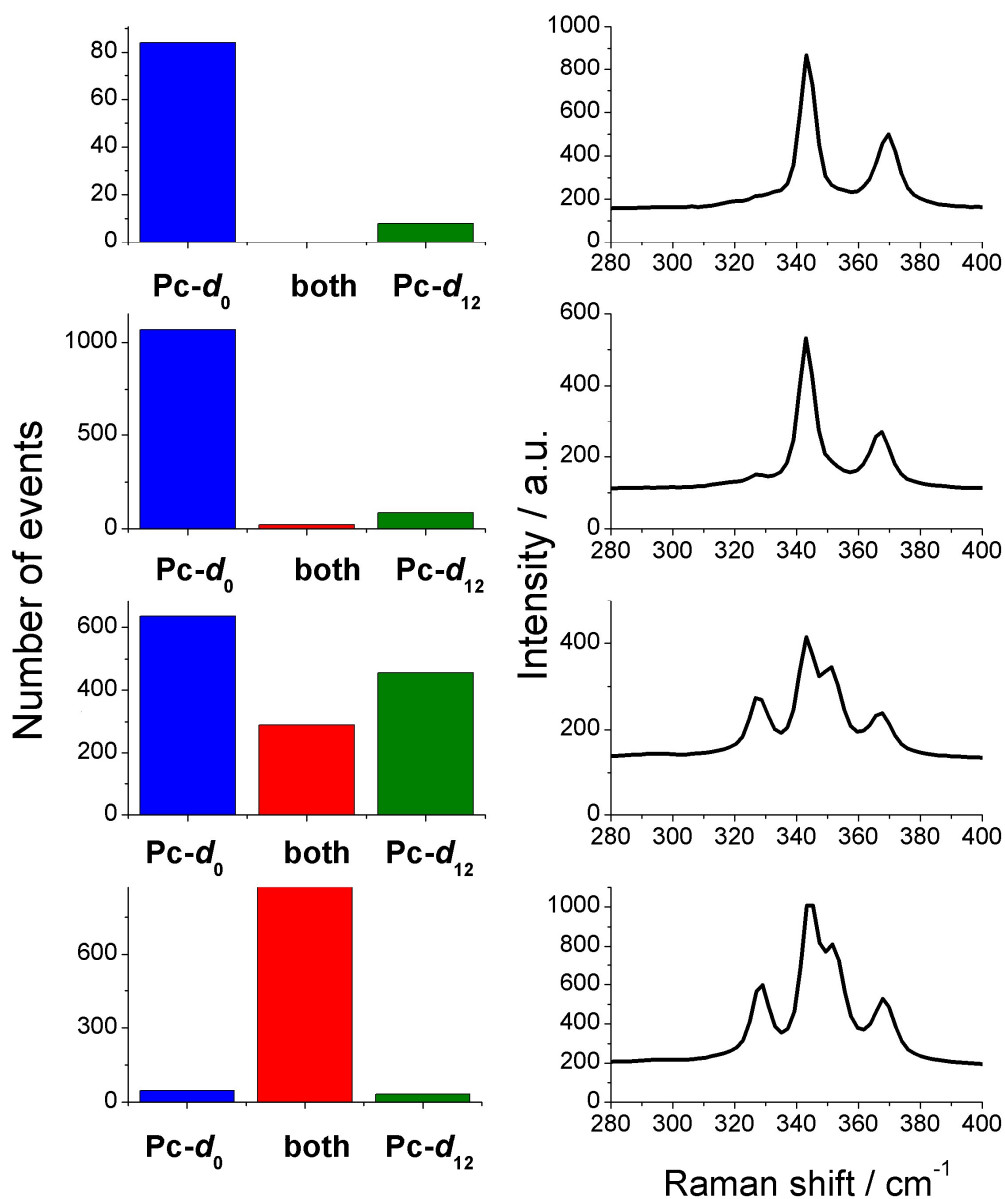
Fig. 3 Left: histograms showing the occurrence of single vs mixed events, obtained for 1:1 Pc-d_0:Pc-d_{12} mixtures of different concentrations deposited on commercial 60x25 nm Au nanorods/glass substrate. From bottom to top: 10^{-7}, 10^{-8}, 10^{-9}, and 10^{-10} M (total concentration of both isotopologues). Right: average spectra obtained for each concentration. 633 nm excitation, 50 µW laser power, 293 K.
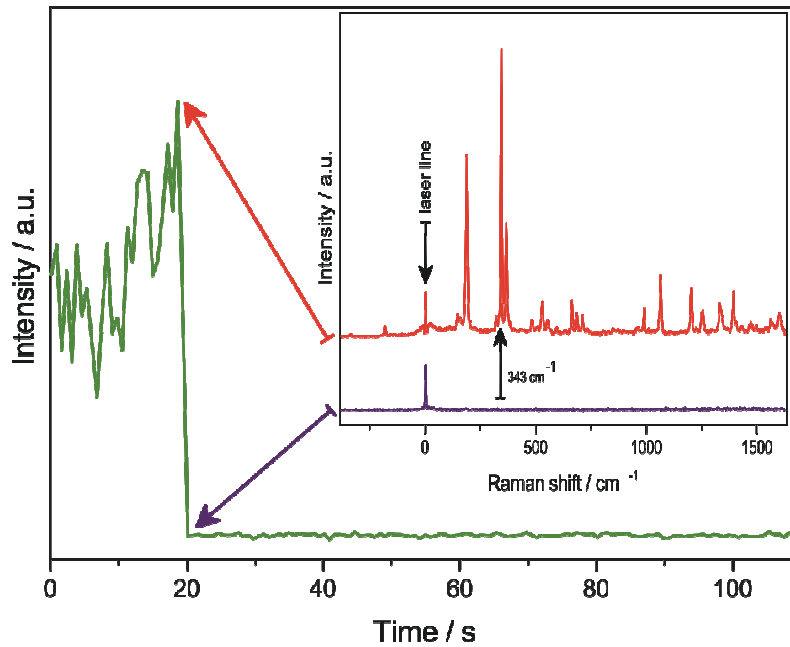
Fig. 4 Time evolution of the integral intensity of the 343 cm^{-1} peak of Pc-d_0, recorded with 0.5 s consecutive exposure times. The inset shows the spectrum just prior to the sudden intensity drop and just after it. Substrate: gold nanostructures electrodeposited on the ITO surface. 633 nm excitation, 50 µW laser power, 293 K.
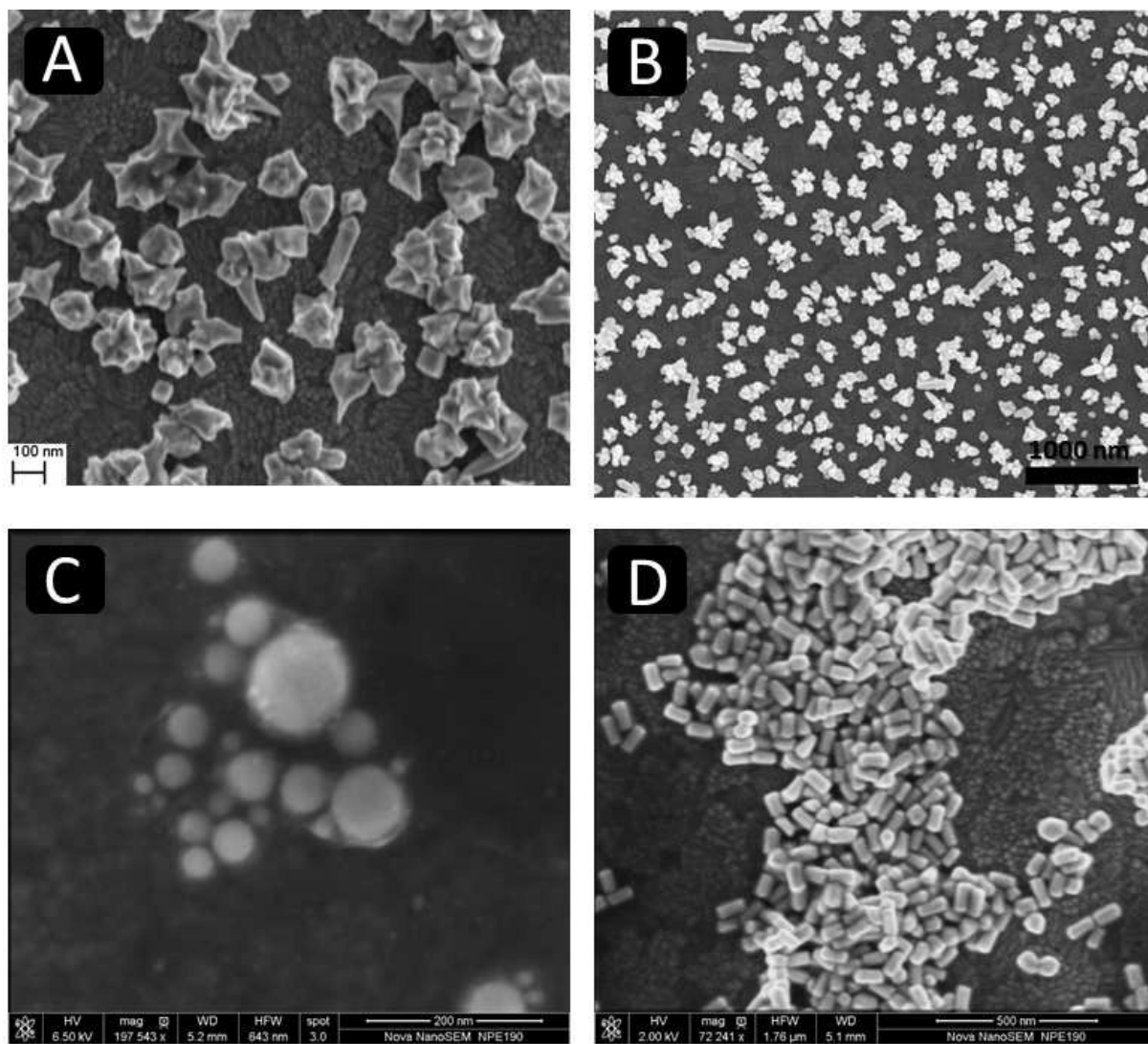
Fig. 5 SEM images of different types of substrates: (A) obtained by electrodeposition at a three-phase junction; (B) obtained by electrorefining using scanning electrochemical microscopy; (C) laser ablated Au nanoparticles; (D) commercial 60x25 nm Au nanorods.
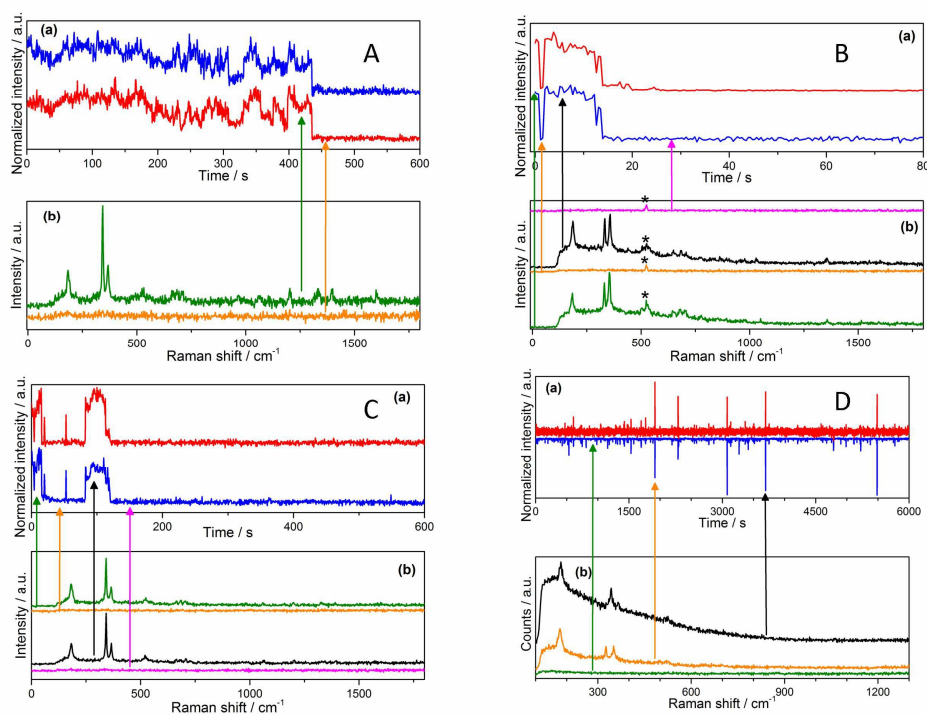
Fig. 6 Time traces of Raman (red) and fluorescence (blue) intensities, and the spectra observed before and after bleaching events. A: Pc-d_0 on gold NPs/glass substrate (250 ms/spectrum, 20 µW laser power). B: Pc-d_{12} on gold NPs/Si substrate; time evolution of the integrated intensities of the 180 cm^{-1} Raman band and of the fluorescence background integrated between 220 and-300 cm^{-1} (200 ms/spectrum, 20 µW laser power). The asterisk marks the 520 cm^{-1} Si (substrate) Raman band. C: Pc-d_0 on gold NPs/Si substrate; time evolution of the integrated intensity of the 365 cm^{-1} Raman band and the integral of the fluorescence background in the range 220-300 cm^{-1} (250 ms/spectrum, 20 µW laser power). D: Pc-d_0 dissolved in gold colloid suspension; time trace of the integrated intensity of the 180 cm^{-1} Raman band and of the integral of the fluorescence background in the range 220-300 cm^{-1} (500 ms/spectrum, 40mW laser power).
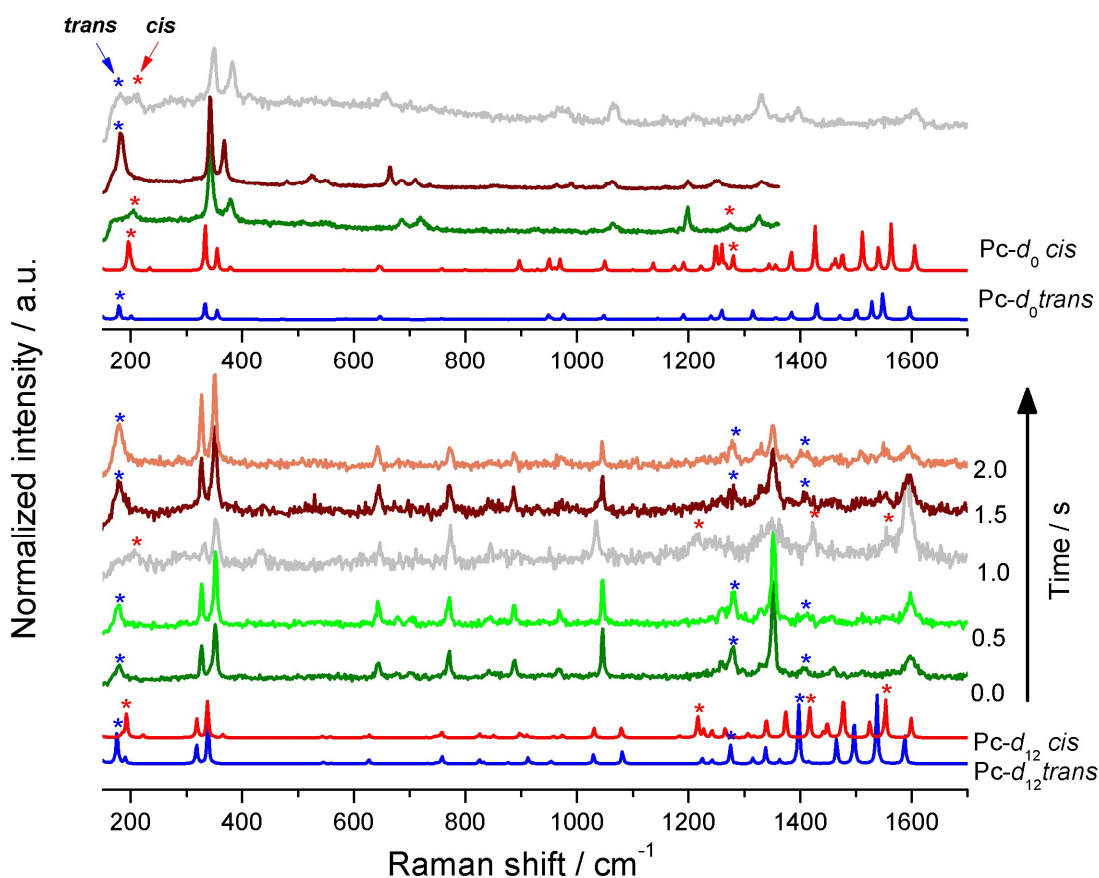
26

Fig. 7 Top, three SMR spectra recorded for Pc-d_0 from different hot spots, compared with theoretical predictions for *trans* (blue) and *cis* (red) tautomeric forms (B3LYP/6-31G(d,p), frequencies scaled by 0.96, intensities corrected for 633 nm excitation and 298 K). The asterisks mark the bands that reveal different frequencies in the two isotopologues. Bottom,consecutive SMR spectra recorded for Pc-d_{12} from the same sample point on Au support, compared with calculated frequencies. Substrate:chemically synthesized Au NPs on glass, 50 µW laser power, 298 K

REFERENCES

1 S. M. Nie and S. R. Emory, *Science*, 1997, **275**, 1102.

2 K. Kneipp, Y. Wang, H. Kneipp, L. T. Perelman, I. Itzkan, R. Dasari and M. S. Feld, *Phys. Rev. Lett.*, 1997, **78**, 1667.

3 M. D. Sonntag, J. M. Klingsporn, L. K. Garibay, J. M. Roberts, J. A. Dieringer, T. Seideman, K. A. Scheidt, L. Jensen, G. C. Schatz and D. R. P. Van, *J. Phys. Chem. C*, 2012, **116**, 478.

4 M. D. Sonntag, D. Chulhai, T. Seideman, L. Jensen and R. P. Van Duyne, *J. Am. Chem. Soc.*, 2013, **135**, 17187.

5 R. Zhang, Y. Zhang, Z. C. Dong, S. Jiang, C. Zhang, L. G. Chen, L. Zhang, Y. Liao, J. Aizpurua, Y. Luo, J. L. Yang and J. G. Hou, *Nature*, 2013, **498**, 82.

6 M. Banik, A. Nag, P. Z. El-Khoury, P. A. Rodriguez, N. Guarrotxena, G. C. Bazan and V. A. Apkarian, *J. Phys. Chem. C*, 2012, **116**, 10415.

7 T. Yano, T. Ichimura, S. Kuwahara, F. H'Dhili, K. Uetsuki, Y. Okuno, P. Verma and S. Kawata, *Nat Commun*, 2013, **4**.

8 S. Yampolsky, D. A. Fishman, S. Dey, E. Hulkko, M. Banik, E. O. Potma and V. A. Apkarian, *Nature Photonics*, 2014, **8**, 650.

9 E. Vogel, M. Köcher, H. Schmickler and J. Lex, *Angew. Chem. Int. Ed. Engl.*, 1986, **25**, 257.

10 S. E. Braslavsky, M. Müller, D. O. Mártire, S. Pörting, S. G. Bertolotti, S. Chakravorti, G. Koç-Weier, B. Knipp and K. Schaffner, *J. Photochem. Photobiol. B-Biology*, 1997, **40**, 191.

11 J. Waluk, in *CRC Handbook of Organic Photochemistry and Photobiology*, ed. M. Oelgemoeller, Griesbeck. A. Ghetti, F., CRC Press, 2012, pp. 809.

12 J. Waluk, M. Müller, P. Swiderek, M. Köcher, E. Vogel, G. Hohlneicher and J. Michl, *J. Am. Chem. Soc.*, 1991, **113**, 5511.

13 J. C. Stockert, M. Cañete, A. Juarranz, A. Villanueva, R. W. Horobin, J. Borrell, J. Teixidó and S. Nonell, *Curr. Med. Chem.*, 2007, **14**, 997.

14 H. Piwoński, C. Stupperich, A. Hartschuh, J. Sepioł, A. Meixner and J. Waluk, *J. Am. Chem. Soc.*, 2005, **127**, 5302.

15 H. Piwoński, A. Hartschuh, N. Urbańska, M. Pietraszkiewicz, J. Sepioł, A. Meixner and J. Waluk, *J. Phys. Chem. C*, 2009, **113**, 11514.

16 H. Piwoński, A. Sokołowski, M. Kijak, S. Nonell and J. Waluk, *J. Phys. Chem. Lett.*, 2013, **4**, 3967−3971.

17 T. Kumagai, F. Hanke, S. Gawinkowski, J. Sharp, K. Kotsis, J. Waluk, M. Persson and L. Grill, *Phys. Rev. Lett.*, 2013, **111**, 246101.

18 T. Kumagai, F. Hanke, S. Gawinkowski, J. Sharp, K. Kotsis, J. Waluk, M. Persson and L. Grill, *Nature Chem.*, 2014, **6**, 41.

19 J. N. Ladenthin, L. Grill, S. Gawinkowski, S. Liu, J. Waluk and T. Kumagai, *ACS Nano*, 2015, DOI: 10.1021/acsnano.5b02147.

20 J. Waluk, *Acc. Chem. Res.*, 2006, **39**, 945.

21 J. Waluk, in *Hydrogen-Transfer Reactions*, eds. J. T. Hynes, J. P. Klinman, H. H. Limbach and R. L. Schowen, Wiley-VCH, Weinheim, 2007, vol. 1, pp. 245.

22 J. Waluk, in *Handbook of Porphyrin Science*, ed. K. Smith, Kadish, K., Guilard, R., World Scientific, Singapore, 2010, vol. 7, p. 359.

23 M. Gil and J. Waluk, *J. Am. Chem. Soc.*, 2007, **129**, 1335.

24 M. Gil, J. Dobkowski, G. Wiosna-Sałyga, N. Urbańska, P. Fita, C. Radzewicz, M. Pietraszkiewicz, P. Borowicz, D. Marks, M. Glasbeek and J. Waluk, *J. Am. Chem. Soc.*, 2010, **132**, 13472.

25 J. Sepioł, Y. Stepanenko, A. Vdovin, A. Mordziński, E. Vogel and J. Waluk, *Chem. Phys. Lett.*, 1998, **296**, 549.

26 A. Vdovin, J. Sepioł, N. Urbańska, M. Pietraszkiewicz, A. Mordziński and J. Waluk, *J. Am. Chem. Soc.*, 2006, **128**, 2577.

27 E. T. Mengesha, J. Sepioł, P. Borowicz and J. Waluk, *J. Chem. Phys.*, 2013, **138**, 174201.

28 A. Vdovin, J. Waluk, B. Dick and A. Slenczka, *ChemPhysChem*, 2009, **10**, 761.

29 S. Gawinkowski, Ł. Walewski, A. Vdovin, A. Slenczka, S. Rols, M. R. Johnson, B. Lesyng and J. Waluk, *Phys.Chem.Chem.Phys.*, 2012, **14**, 5489.

30 K. Malsch and G. Hohlneicher, *J. Phys. Chem. A*, 1997, **101**, 8409.

31 A. Starukhin, E. Vogel and J. Waluk, *J. Phys. Chem. A*, 1998, **102**, 9999.

32 E. T. Mengesha, A. Zehnacker-Rentien, J. Sepioł, M. Kijak and J. Waluk, *J. Phys. Chem. B*, 2014.

33 E. C. Le Ru, M. Meyer and P. G. Etchegoin, *J. Phys. Chem. B*, 2006, **110**, 1944.

34 P. G. Etchegoin, M. Meyer, E. Blackie and E. C. Le Ru, *Anal. Chem.*, 2007, **79**, 8411.

35 J. A. Dieringer, R. B. Lettan, K. A. Scheidt and R. P. Van Duyne, *J. Am. Chem. Soc.*, 2007, **129**, 16249.

36 E. Blackie, E. C. Le Ru, M. Meyer, M. Timmer, B. Burkett, P. Northcote and P. G. Etchegoin, *PCCP*, 2008, **10**, 4147.

37 P. J. G. Goulet and R. F. Aroca, *Anal. Chem.*, 2007, **79**, 2728.

38 Y. Sawai, B. Takimoto, H. Nabika, K. Ajito and K. Murakoshi, *J. Am. Chem. Soc.*, 2007, **129**, 1658.

39 P. G. Etchegoin, E. C. Le Ru and A. Fainstein, *PCCP*, 2011, **13**, 4500.

40 R. D. Deegan, O. Bakajin, T. F. Dupont, G. Huber, S. R. Nagel and T. A. Witten, *Nature*, 1997, **389**, 827.

41 B. C. Stipe, M. A. Rezaei and W. Ho, *Phys. Rev. Lett.*, 1999, **82**, 1724.

42 F. Buchner, J. Xiao, E. Zillner, M. Chen, M. Rockert, S. Ditze, M. Stark, H. P. Steinruck, J. M. Gottfried and H. Marbach, *J. Phys. Chem. C*, 2011, **115**, 24172.

43 F. Buchner, E. Zillner, M. Rockert, S. Glassel, H. P. Steinruck and H. Marbach, *Chem. Eur. J.*, 2011, **17**, 10226.

44 M. Eichberger, M. Marschall, J. Reichert, A. Weber-Bargioni, W. Auwarter, R. L. C. Wang, H. J. Kreuzer, Y. Pennec, A. Schiffrin and J. V. Barth, *Nano Lett.*, 2008, **8**, 4608.

45 H. Marbach and H. P. Steinruck, *Chem. Commun.*, 2014, **50**, 9034.

46 G. Rojas, X. Chen, C. Bravo, J. H. Kim, J. S. Kim, J. Xiao, P. A. Dowben, Y. Gao, X. C. Zeng, W. Choe and A. Enders, *J Phys Chem C*, 2010, **114**, 9408.

47 E. Cortés, P. G. Etchegoin, E. C. Le Ru, A. Fainstein, M. E. Vela and R. C. Salvarezza, *J. Am. Chem. Soc.*, 2010, **132**, 18034.

48 C. Artur, R. E. C. Le and P. G. Etchegoin, *J. Phys. Chem. Lett.*, 2011, **2**, 3002.

49 E. C. Le Ru, E. Blackie, M. Meyer and P. G. Etchegoin, *J. Phys. Chem. C*, 2007, **111**, 13794.

50 Y. Suzaki and A. Tachibana, *Appl. Opt.*, 1975, **14**, 2809.

51 E. C. Le Ru, L. C. Schroeter and P. G. Etchegoin, *Anal. Chem.*, 2012, **84**, 5074.

52 A. Reigue, B. Auguie, P. G. Etchegoin and E. C. Le Ru, *J. Raman Spectrosc.*, 2013, **44**, 573.

53 B. Auguie, A. Reigue, E. C. Le Ru and P. G. Etchegoin, *Anal. Chem.*, 2012, **84**, 7938.

54 E. J. Blackie, E. C. Le Ru and P. G. Etchegoin, *J. Am. Chem. Soc.*, 2009, **131**, 14466.

55 H. X. Xu, J. Aizpurua, M. Kall and P. Apell, *Phys Rev E*, 2000, **62**, 4318.

56 E. Hao and G. C. Schatz, *J. Chem. Phys.*, 2004, **120**, 357.

57 G. C. Schatz, M. A. Young and R. P. Van Duyne, *Surface-Enhanced Raman Scattering: Physics and Applications*, 2006, **103**, 19.

58 S. M. Barnett, N. Harris and J. J. Baumberg, *Phys. Chem. Chem. Phys.*, 2014, **16**, 6544.

59 S. Buchanan, R. E. C. Le and P. G. Etchegoin, *Phys. Chem. Chem. Phys.*, 2009, **11**, 7406.

60 Y. Gao and T. López-Ríos, *Surf. Sci.*, 1985, **162**, 976.

61 J. T. Hugall and J. J. Baumberg, *Nano Lett.*, 2015.

62 K. Ikeda, S. Suzuki and K. Uosaki, *J. Am. Chem. Soc.*, 2013, **135**, 17387.

63 S. Mahajan, R. M. Cole, J. D. Speed, S. H. Pelfrey, A. E. Russell, P. N. Bartlett, S. M. Barnett and J. J. Baumberg, *The Journal of Physical Chemistry C*, 2010, **114**, 7242.

64 P. Ciąćka, P. Fita, A. Listkowski, M. Kijak, S. Nonell, D. Kuzuhara, H. Yamada, C. Radzewicz and J. Waluk, *J. Phys. Chem. B*, 2014.

65 K. Ray and J. R. Lakowicz, *J Phys Chem C*, 2013, **117**, 15790.

66 A. Parfenov, I. Gryczynski, J. Malicka, C. D. Geddes and J. R. Lakowicz, *J. Phys. Chem. B*, 2003, **107**, 8829.

67 I. Gryczynski, J. Malicka, Y. B. Shen, Z. Gryczynski and J. R. Lakowicz, *J. Phys. Chem. B*, 2002, **106**, 2191.

68 X. X. Han, Y. Kitahama, Y. Tanaka, J. Guo, W. Q. Xu, B. Zhao and Y. Ozaki, *Anal. Chem.*, 2008, **80**, 6567.

69 C. C. Lin, Y. M. Yang, Y. F. Chen, T. S. Yang and H. C. Chang, *Biosensors & Bioelectronics*, 2008, **24**, 178.

70 S. Schlucker, *ChemPhysChem*, 2009, **10**, 1344.

71 J. V. Pellegrotti, G. P. Acuna, A. Puchkova, P. Holzmeister, A. Gietl, B. Lalkens, F. D. Stefani and P. Tinnefeld, *Nano Lett.*, 2014, **14**, 2831.

72 Y. D. Zhao, Y. Z. Xie, Z. Y. Bao, Y. H. Tsang, L. M. Xie and Y. Chai, *J Phys Chem C*, 2014, **118**, 11827.

73 P. G. Etchegoin, E. C. Le Ru, R. C. Maher and L. F. Cohen, *PCCP*, 2007, **9**, 4923.

74 P. G. Etchegoin, P. D. Lacharmoise and E. C. Le Ru, *Anal. Chem.*, 2009, **81**, 682.

75 M. Kanehara, H. Takahashi and T. Teranishi, *Angew. Chem. Int. Edit.*, 2008, **47**, 307.

76 N. Urbańska, M. Pietraszkiewicz and J. Waluk, *J. Porphyrins Phthalocyanines*, 2007, **11**, 596.

77 N. Leopold and B. Lendl, *J. Phys. Chem. B*, 2003, **107**, 5723.

78 W. Nogala, P. Kannan, S. Gawinkowski, M. Jonsson-Niedziolka, M. Kominiak, J. Waluk and M. Opallo, *Nanoscale*, 2015, **7**, 10767.

79 I. Kamińska, M. Jönsson-Niedziółka, A. Kamińska, M. Pisarek, R. Hołyst, M. Opałło and J. Niedziółka-Jönsson, *J. Phys. Chem. C*, 2012, **116**, 22476.

80 M. M. Brust, M. Walker, D. Bethell, D. J. Schiffrin and R. J. Whyman, *J. Chem. Soc. Chem. Commun.* , 1994, 801.

81 *Gaussian 09, Revision B.01*, M. J. Frisch, *et al.*, Gaussian, Inc., Wallingford CT, 2010.